Available online at www.sciencedirect.com
SCIENCE DIRECT
Journal of Magnetic Resonance 179 (2006) 190–198
JMR Journal of Magnetic Resonance
www.elsevier.com/locate/jmr

Intensity and mosaic spread analysis from PISEMA tensors in solid-state NMR

J.R. Quine [a,b,*], S. Achuthan [a], T. Asbury [c], R. Bertram [a,c], M.S. Chapman [c,d], J. Hu [e], T.A. Cross [b,d]

[a] Department of Mathematics, Florida State University, Tallahassee, FL 32306-4510, USA
[b] National High Magnetic Field Laboratory, Tallahassee, FL 32310, USA
[c] Institute of Molecular Biophysics, Florida State University, Tallahassee, FL 32306, USA
[d] Department of Chemistry and Biochemistry, Florida State University, Tallahassee, FL 32306, USA
[e] NIDDK, NIH, Bethesda, MD 20892, USA

Received 7 September 2005; revised 1 December 2005
Available online 18 January 2006

Abstract

The solid-state NMR experiment PISEMA, is a technique for determining structures of proteins, especially membrane proteins, from oriented samples. One method for determining the structure is to find orientations of local molecular frames (peptide planes) with respect to the unit magnetic field direction, $\mathbf{B}_0$. This is done using equations that compute the coordinates of this vector in the frames. This requires an analysis of the PISEMA function and its degeneracies. As a measure of the sensitivity of peptide plane orientations to the data, we use these equations to derive a formula for the intensity function in the powder pattern. With this function and other measures, we investigate the effect of small changes in peptide plane orientations depending on the location of the resonances in the powder pattern spectrum. This gives us an indication of the change in lineshape due to mosaic spread and a way to interpret these in terms of an orientational error bar.

Keywords: PISEMA tensors; Solid-state NMR; Powder pattern intensity; Mosaic spread; Lineshapes

1. Introduction

Membrane proteins form an important class of proteins in all genomes [1]. The application of solid-state nuclear magnetic resonance (ssNMR) spectroscopy to aligned samples has proved to be a successful technique for the determination of the three-dimensional structure of these proteins [2–6]. One such ssNMR experiment is PISEMA, polarization inversion spin exchange at magic angle [12,13]. This two-dimensional (2D) NMR experiment gives the anisotropic ^{15}N chemical shift and the ^{15}N–^{1}H dipolar coupling for each labelled residue, providing information on the orientation of peptide planes relative to the direction of an external magnetic field. This information can then be used to construct a model of the protein [6–11]. Determining the orientation of a local molecular frame is equivalent to finding the coordinates of $\mathbf{B}_0$ in the frame [15] so it is important to know how well the coordinates are determined by the data.

The aim of this paper is to quantify the sensitivity of the calculated coordinates of $\mathbf{B}_0$ to small changes or errors in experimental PISEMA measurements. As one measure, we use powder pattern intensity. The powder pattern consists of data points for all possible orientations [16]. Formulas for the intensity can be computed from the gradients of the expressions for frequency as a function of $\mathbf{B}_0$. The shape and intensity of 2D NMR powder patterns has been investigated in detail in [14] and our analysis for PISEMA involves a special case where one of the tensors (dipolar) is traceless and symmetric.

* Corresponding author. Fax: +1 850 644 4053.
E-mail address: quine@math.fsu.edu (J.R. Quine).

1090-7807/$ - see front matter © 2005 Elsevier Inc. All rights reserved.
doi:10.1016/j.jmr.2005.12.002

We compute an explicit formula for the intensity using the Jacobian of the PISEMA transformation and relate this to the sensitivity of the computed structure on the data. The formula for intensity is completely general, with the principal values and the relative tensor orientations appearing as parameters. To avoid the problem of scaling in the frequency plane, we focus on the relative intensity between pairs of points. We also do some computation on the effect of small changes in $\mathbf{B}_0$ on the chemical shift and dipolar frequencies separately.

In these investigations degeneracies (or ambiguities) [16,17] are encountered when solving for $\mathbf{B}_0$ from PISEMA data. We derive an explicit formula for each of the degeneracies as a sequence of signs ± 1. We relate this sequence of signs to the position of the data point in the powder pattern.

As an illustration, we examine data from the M2 transmembrane domain (L26–L43) in a lipid bilayer [6]. In this example most of the data lie within low intensity regions of the powder pattern, indicating that the structure obtained from the PISEMA data will be robust to small errors in the data while conversely, the linewidth due to mosaic spread may be large.

2. Theory

2.1. Coordinate frames

To determine the coordinates of $\mathbf{B}_0$, it is necessary to specify the reference coordinate frame. Often the choice is the principal axis frame of the ^{15}N chemical shift tensor [16,17,19–21]. For the present analysis, the equations are simpler when the principal axis frame of the ^{15}N–^{1}H dipolar coupling tensor (NH dipolar tensor) is used.

We first describe these two frames. Both the dipolar and chemical shift tensors are fixed with respect to the peptide plane. Both have the first and third vectors in the peptide plane with the second vector a peptide plane normal chosen in the direction $\overrightarrow{\mathrm{CN}} \times \overrightarrow{\mathrm{NC}\alpha}$ [16,21,22].

The NH dipolar tensor principal axis frame has the first vector in the direction of the NH bond, the third vector perpendicular to the first in the peptide plane. The principal axis frame for the chemical shift of the nitrogen is ($\boldsymbol{\sigma}_{11}$, $\boldsymbol{\sigma}_{22}$, $\boldsymbol{\sigma}_{33}$) with major principal axis as the third vector. The coordinates of $\mathbf{B}_0$ in the principal axis frame for the chemical shift are denoted by x, y, z, and in the principal axis frame for the NH dipolar tensor by u, y, v. Note that the coordinate y is the same in both frames.

The relationship between the two frames is given by the angle β,

$$\begin{aligned} x &= u\sin\beta + v\cos\beta \\ z &= u\cos\beta - v\sin\beta \end{aligned} \tag{1}$$

where β is the angle from $\boldsymbol{\sigma}_{33}$ to the NH bond direction around the peptide plane normal (Fig. 1). Experiments show that β is approximately 17° [18].

2.2. PISEMA equations

The observables in the PISEMA experiment are the chemical shift of the ^{15}N frequency (ppm) and the magnitude of the splitting of this signal by the dipolar coupling to the bonded hydrogen (kHz). We write equations for the chemical shift σ and dipolar splitting ν in the principal axis frame of the dipolar tensor, and we assume that the sign of ν can be determined (i.e, there is no sign degeneracy).

Suppose $\sigma_{33} > \sigma_{22} > \sigma_{11}$ are the principal values of the chemical shift tensor. Then the PISEMA equations [16] in the principal axis frame of the chemical shift tensor are

$$\begin{aligned} \sigma &= \sigma_{11}x^2 + \sigma_{22}y^2 + \sigma_{33}z^2 \\ \nu &= \frac{\nu_\parallel}{2}\left(3(x\sin\beta + z\cos\beta)^2 - 1\right). \end{aligned} \tag{2}$$

Substituting for x and z using (1) in (2), the PISEMA equations in the dipolar frame turn out to be

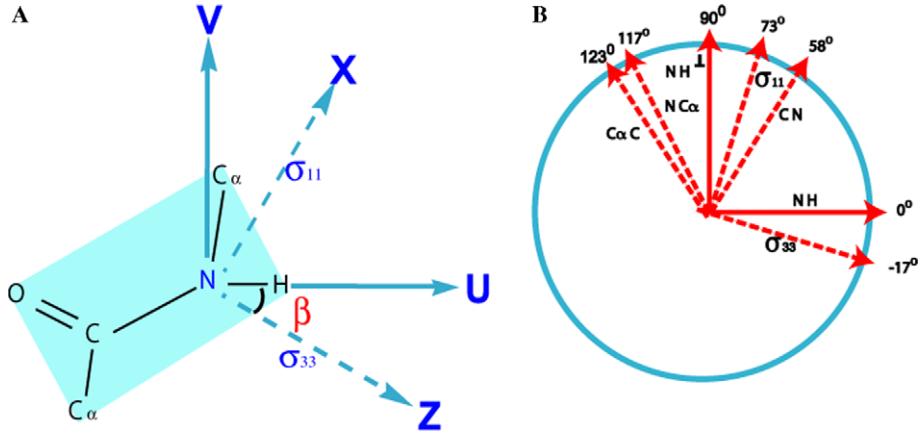

Fig. 1. (A) Vectors in the peptide plane. We assume that the principal axis directions $\boldsymbol{\sigma}_{11}$ and $\boldsymbol{\sigma}_{33}$ for the chemical shift are in the peptide plane. (B) Angles [11,19] made relative to the NH vector when $\beta = -17°$.

$$\sigma - \sigma_{22} = au^2 + 2buv + cv^2$$
$$\frac{2v + v_\parallel}{3v_\parallel} = u^2 \tag{3}$$

where

$$a = \sigma_{11}\sin^2\beta + \sigma_{33}\cos^2\beta - \sigma_{22},$$
$$b = (\sigma_{11} - \sigma_{33})\sin\beta\cos\beta, \tag{4}$$
$$c = \sigma_{11}\cos^2\beta + \sigma_{33}\sin^2\beta - \sigma_{22}.$$

In deriving (3), we use the relationship between the coordinates of $\mathbf{B}_0$ in the dipolar frame, i.e.,

$$u^2 + y^2 + v^2 = 1. \tag{5}$$

If $\beta = 17°$ and $\sigma_{11} \approx 30$ ppm, $\sigma_{22} \approx 50$ ppm, $\sigma_{33} \approx 200$ ppm, then $a \approx 135$ ppm, $b \approx -48$ ppm, and $c \approx -5$ ppm with a positive, b and c negative.

We also define the discriminant by

$$f = b^2 - ac. \tag{6}$$

2.3. The PISEMA function and its inverse

Eq. (3) give a transformation from the $\mathbf{B}_0$ sphere $u^2 + y^2 + v^2 = 1$ into the frequency plane (σ, v). The transformation is the *PISEMA function* [16] and the image is the (*singlet*) *powder pattern*.

2.3.1. The PISEMA function simplified

From now onwards, we use $\tilde{\sigma} = \sigma - \sigma_{22}$ and $\tilde{v} = \frac{2v+v_\parallel}{3v_\parallel}$. Our $\tilde{\sigma}$ is not the same as that in [16].

Eq. (3) is further simplified by the introduction of new variables

$$w = bu + cv$$
$$\zeta = c\tilde{\sigma} + f\tilde{v}. \tag{7}$$

Now (3) simplifies to

$$\zeta = w^2$$
$$\tilde{v} = u^2. \tag{8}$$

From (8) it follows that the eight points

$$(\pm u, \pm y, \pm w) \tag{9}$$

give the same values for $\tilde{\sigma}$ and $\tilde{v}$. The existence of multiple solutions is referred to as a *degeneracy* or *ambiguity*. As we show below, depending on $\tilde{\sigma}$ and $\tilde{v}$ there may be only four of these solutions corresponding to points $\mathbf{B}_0$ on the sphere.

2.3.2. Inverse of the PISEMA function and degeneracies

To solve for $\mathbf{B}_0$ from the data, the PISEMA function needs to be inverted. This was done in [16] in terms of degeneracies $\{\varepsilon_1, \varepsilon_2, \varepsilon_3, \varepsilon_4\}$ for the coordinates of $\mathbf{B}_0$ in the principal axis frame of the chemical shift tensor. Since we are assuming that the sign of the dipolar is resolved we are considering $\varepsilon_1 = 1$. In terms of these degeneracies using (5), (7), and (8), the inverse in our reference frame can be shown to be:

$$u = \varepsilon_2\sqrt{\tilde{v}}$$
$$w = \varepsilon_3\sqrt{\zeta}$$
$$y = \varepsilon_4\sqrt{\frac{1}{c^2}\left[c^2 - (c^2 + b^2)\tilde{v} - \zeta + 2\varepsilon_2\varepsilon_3 b\sqrt{\tilde{v}\zeta}\right]}. \tag{10}$$

2.4. The PISEMA powder pattern

The PISEMA powder pattern is the image of the disk $u^2 + v^2 \leqslant 1$ under (3) (see Fig. 2). From (8) it follows that the powder pattern is in the sector

$$\tilde{v} \geqslant 0 \quad \zeta \geqslant 0. \tag{11}$$

The powder pattern can be described as the union of the interior of an ellipse and the interior of a triangle with one elliptical side (see Fig. 2). As shown below, in some cases of interest the triangle can be very small, smaller than in (Fig. 2).

The σ, v coordinates of points Q, S_2 shown in (Fig. 2) are:

$$Q = (\sigma_{22}, \frac{-v_\parallel}{2})$$
$$S_2 = \frac{1}{b^2 + c^2}\left(-fc + \sigma_{22}(b^2 + c^2), \frac{(2c^2 - b^2)v_\parallel}{2}\right). \tag{12}$$

2.4.1. The PISEMA ellipse

The inequality $u^2 + v^2 \leqslant 1$ becomes, using the third equation in (10)

$$\zeta + \tilde{v}(b^2 + c^2) - c^2 \leqslant 2b\varepsilon_2\varepsilon_3\sqrt{\zeta\tilde{v}}. \tag{13}$$

The equation $u^2 + v^2 = 1$ becomes

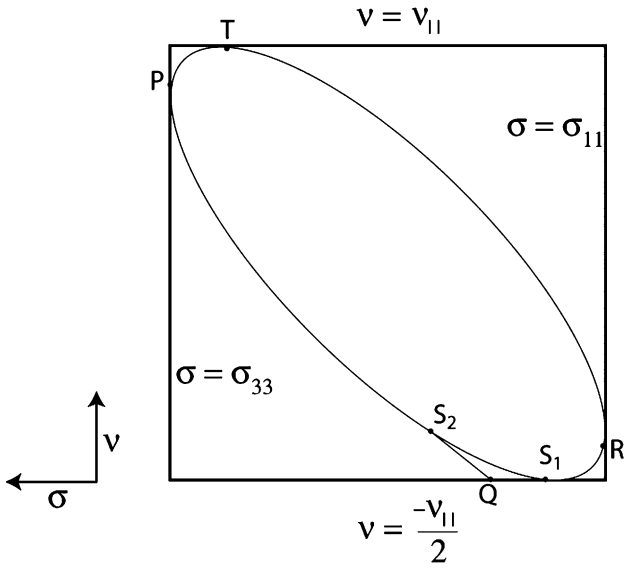

Fig. 2. The PISEMA powder pattern. The ellipse is enclosed in a rectangle with sides as indicated. The σ, v coordinates of points shown is given in (12) and in [16]. The tangent line QS_2 is given by $c(\sigma - \sigma_{22}) = -f(\frac{2v+v_\parallel}{3v_\parallel})$. Following NMR conventions, the positive direction for the σ axis points to the left.

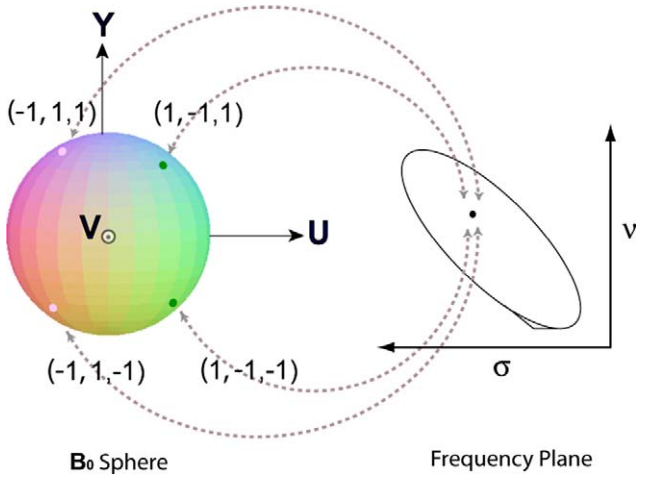

Fig. 3. Degeneracies of the PISEMA function. There are four possible points $\mathbf{B}_0$ corresponding to the point shown within the ellipse in the frequency plane. These correspond to an appropriate choice of $(\varepsilon_2,\varepsilon_3,\varepsilon_4)$ as shown in the figure. Here σ is the chemical shift and ν is the dipolar interaction frequency.

$$\left(\zeta+\tilde{\nu}(b^2+c^2)-c^2\right)^2=4b^2\zeta\tilde{\nu} \tag{14}$$

and this is the equation of the *PISEMA ellipse*. Thus when $\mathbf{B}_0$ is in the peptide plane, the corresponding point in the frequency plane is on the ellipse. The ellipse with interior is given by

$$\left(\zeta+\tilde{\nu}(b^2+c^2)-c^2\right)^2\leqslant 4b^2\zeta\tilde{\nu}. \tag{15}$$

In case $b<0$ Eqs. (15) and (13) show that for points within the ellipse, inequality (15) can hold only if $\varepsilon_2\varepsilon_3=-1$. Thus within the PISEMA ellipse $\varepsilon_2=-\varepsilon_3$ and there are at most two possible solutions of (10) (thus at most four points on the $\mathbf{B}_0$ sphere, see Fig. 3).

In Fig. 4 the two solid lines divide the disk into four sectors given by $(\varepsilon_2,\varepsilon_3)$ equal to $(1,1)$, $(1,-1)$, $(-1,1)$, $(-1,-1)$. The two large sectors correspond to $(1,-1)$ and $(-1,1)$ and the analysis above shows that points mapping to the ellipse are in these two sectors. Below we show that part of these sectors is also mapped outside the ellipse.

Transforming Eq. (14) of the ellipse into standard form, it can be shown that

$$\text{area of PISEMA ellipse}=\iint\limits_{\substack{\text{PISEMA}\\ \text{ellipse}}}\mathrm{d}\tilde{\sigma}\,\mathrm{d}\tilde{\nu}=\frac{\pi|b|}{2}. \tag{16}$$

2.4.2. The PISEMA triangle

Using (14), we see that the lines $\tilde{\nu}=0$ and $\zeta=0$ are tangent to the ellipse at the points S_1 and S_2 (Fig. 2). The sector $\tilde{\nu}\geqslant 0$, $\zeta\geqslant 0$ outside the ellipse is called the *PISEMA triangle*.

2.4.3. Points mapping to the triangle

The lines $bu+cv=0$ and $u=0$ map to sides QS_2 and QS_1, respectively, of the PISEMA triangle (see Fig. 2). This triangle has one curved edge from S_1 to S_2 which is the image of the part of the circle $u^2+v^2=1$ in the sector $w=bu+cv\leqslant 0$, $u\leqslant 0$. Write $u^2+v^2=1$ as

$$u^2+\left[\frac{w-bu}{c}\right]^2=1.$$

Eq. (8) shows that leaving w fixed and changing the sign of u does not change the image under the PISEMA function. Thus

$$u^2+\left[\frac{w+bu}{c}\right]^2=1 \tag{17}$$

also maps onto the curved edge of the triangle. This is an ellipse (dashed ellipse in Fig. 4). The region inside the circle and the dotted ellipse maps onto the PISEMA triangle. This large area mapping onto the small triangle indicates the possibility of a large error. The error can be quantified locally using an intensity function.

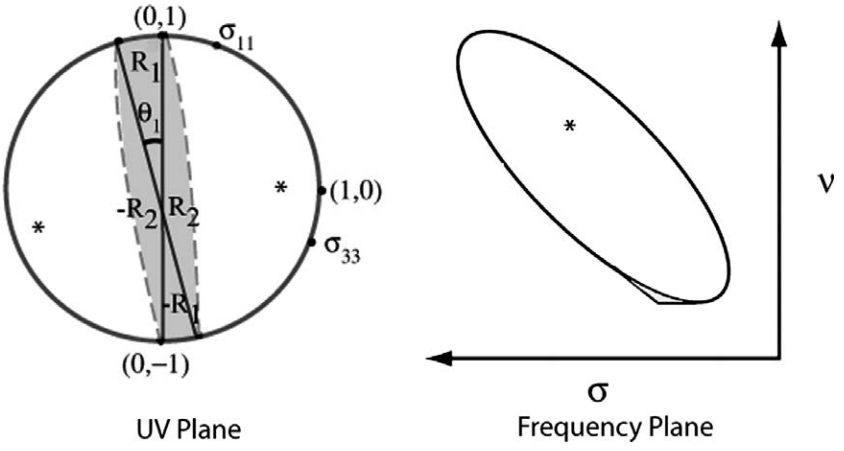

Fig. 4. Regions $\pm R_1$ and $\pm R_2$ in the u,v plane map to the PISEMA triangle. The points $\boldsymbol{\sigma}_{11}$ and $\boldsymbol{\sigma}_{33}$ on the boundary of the disk are principal axis directions for the chemical shift tensor. The region inside the dashed ellipse maps to the PISEMA triangle. The diagonal line is given by $w=bu+cv=0$ or in polar coordinates by $\theta=\theta_1=\arctan|c/b|$. The points labelled $*$ map onto the sweet spot.

2.5. Powder pattern intensity

We define the intensity of a region in the powder pattern as the proportion of the area on the $\mathbf{B}_0$ sphere that maps onto the region. It is one measure of the sensitivity of the coordinates of $\mathbf{B}_0$ to error in the data. The higher the intensity, the greater the possibility of error in $\mathbf{B}_0$.

The local intensity is computed from the Jacobian of the PISEMA function. Suppose the $\mathbf{B}_0$ sphere is normalized so that the total area is 1, then

$$d\Omega = \frac{1}{2\pi|y|}\,du\,dv \tag{18}$$

is the infinitesimal area from the two points on the $\mathbf{B}_0$ sphere $(u, \pm y, v)$. By taking the Jacobian of the transformation (3) we get

$$d\tilde{\sigma}\,d\tilde{\nu} = 4|uw|\,du\,dv \tag{19}$$

and by (18) and (19), the intensity from the two points is

$$\text{Intensity} = \frac{d\Omega}{d\tilde{\sigma}d\tilde{\nu}} = \frac{1}{8\pi|uwy|}. \tag{20}$$

The intensity is infinite at points on the ellipse ($y = 0$) and on the straight line edges of the PISEMA triangle ($w = 0$ and $u = 0$). In the first case ($y = 0$), $\mathbf{B}_0$ is in the peptide plane.

Using (10) and substituting for u, w, and y, the intensity function (20) can be written as a function in the frequency plane

$$\text{Intensity}^{\varepsilon}(\tilde{\sigma},\tilde{\nu}) = \frac{|c|}{8\pi}\left(c^2\tilde{\nu}\zeta - (c^2+b^2)(\tilde{\nu})^2\zeta - \tilde{\nu}\zeta^2 + 2\varepsilon b(\tilde{\nu}\zeta)^{\frac{3}{2}}\right)^{-\frac{1}{2}} \tag{21}$$

where the superscript $\varepsilon = \varepsilon_2\varepsilon_3 = \pm 1$.

At a point inside the ellipse $\varepsilon = -1$ and

$$d\Omega = 2\,\text{Intensity}^{-}\,d\tilde{\sigma}\,d\tilde{\nu} \tag{22}$$

where (20) has been multiplied by two since each point in the ellipse corresponds to two points in the circle. The total intensity for a region in the ellipse is obtained by integrating (22) over the region, or equivalently by integrating (20) over the region in the (u, v) plane which maps onto it.

For a region in the PISEMA triangle the contributions for $\varepsilon = \pm 1$ should be added,

$$d\Omega = 2(\text{Intensity}^{+} + \text{Intensity}^{-})d\tilde{\sigma}\,d\tilde{\nu}. \tag{23}$$

The level curves for intensity have been plotted in Fig. (5). The figure also shows the point of minimum intensity at $(\sigma, v) = (136, 5.26)$. This point is called the *sweet spot* (see below). There is a rapid increase in intensity as the boundary is approached.

Intensity is related to the ratio of the magnitudes of changes on the $\mathbf{B}_0$ sphere to changes in the frequency plane. The change in frequency can be interpreted as error in the determination of the spectral peak.

More precisely, let

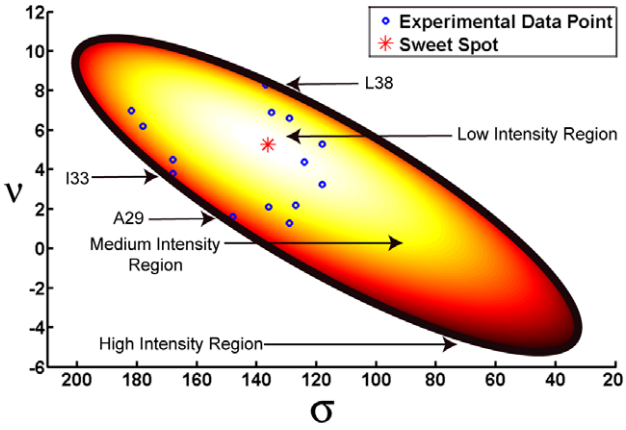

Fig. 5. A contour plot of the intensity within the PISEMA ellipse. The intensity is small near the ellipse center, and large near the edge. A star denotes the point of minimum intensity, the *sweet spot*. Data points for M2 are indicated with circles. For the chemical shift principal values and β angle used here the triangle is too small to be seen.

$$ds^2_{\mathbf{B}_0} = du^2 + dv^2 + dy^2 \quad ds^2_{\tilde{\sigma}\tilde{\nu}} = d\tilde{\sigma}^2 + d\tilde{\nu}^2. \tag{24}$$

The intensity

$$\frac{d\Omega}{d\tilde{\sigma}d\tilde{\nu}} = \left(\frac{ds_{\mathbf{B}_0}}{ds_{\tilde{\sigma}\tilde{\nu}}}\right)_{\max}\left(\frac{ds_{\mathbf{B}_0}}{ds_{\tilde{\sigma}\tilde{\nu}}}\right)_{\min} \tag{25}$$

is the product of the maximum and minimum ratios $ds_{\mathbf{B}_0}/ds_{\tilde{\sigma}\tilde{\nu}}$ at a point. If the intensity is large at a point in the frequency plane, there can be a direction with a large error in the determination of the coordinates of $\mathbf{B}_0$. A complete analysis of the error requires an analysis of the dependence of error on the direction of the error vector. In the section on mosaic spread below, we analyze the error for σ and v separately at several data points.

To properly interpret $ds_{\tilde{\sigma}\tilde{\nu}}$, which is a combination of chemical shift and dipolar error, σ and v should be scaled so that the experimental error is roughly the same for both observables. In the analysis below we take the ratio of intensities at two points, so this scaling cancels out and will not affect the result.

2.6. Intensity and area of the PISEMA ellipse and triangle

The PISEMA triangle has very small area in relation to the area of the powder pattern, but the intensity there is significant. This indicates the possibility of large error if the data point is in the triangle. The calculations are sketched below.

2.6.1. Area of the triangle

In the following, the area of the PISEMA triangle is computed. The sector $u > 0$, $bu + cv < 0$ ($\varepsilon_2 > 0, \varepsilon_3 < 0$) of the circle maps once onto the powder pattern. The area of the powder pattern can be obtained by integrating (19) over this sector. The resulting area is

$$\text{area of powder pattern} = \int_{\text{powder}}\int_{\text{pattern}} d\tilde{\sigma}\, d\tilde{\nu} = \frac{1}{2}(|c| + |b|(\pi - \theta_1)) \quad (26)$$

where $\theta_1 = \arctan|c/b|$. Since from (16) the area inside the ellipse is $\pi|b|/2$, it follows that

$$\text{area of triangle} = \tfrac{1}{2}(|c| - |b|\theta_1). \quad (27)$$

2.6.2. Intensity of the triangle

From (Fig. 4), the intensity of the PISEMA triangle is

$$2\int_{R_1}\int d\Omega + 2\int_{R_2}\int d\Omega. \quad (28)$$

In polar coordinates,

$$d\Omega = \frac{1}{2\pi}\frac{r\,dr\,d\theta}{\sqrt{1-r^2}}. \quad (29)$$

The integral over R_1 can be found in closed form,

$$\int_{R_1}\int d\Omega = \frac{1}{2\pi}\theta_1. \quad (30)$$

The integral over R_2 does not have a convenient closed form, but (17) gives an explicit equation for the boundary of R_2 and the integral can be done numerically.

3. Discussion

3.1. Numerical computation

Results are shown in the case where

$$\sigma_{11} = 31\text{ppm} \quad \sigma_{22} = 55\text{ppm} \quad \sigma_{33} = 202\text{ppm} \quad \beta = 17^\circ.$$

Using (4) we obtain

$$a = 132\text{ppm} \quad b = -48\text{ppm} \quad c = -9\text{ ppm} \quad f = 3504.$$

The angle θ_1 in (30) is .19 radians (11°) and the integral (30) is .03. The integral of $d\Omega$ over R_2 is computed using numerical integration to be .02. Thus by (28) the total intensity for the region of the powder pattern outside the ellipse is $2(.03 + .02) = .1$ or 10%, consistent with an earlier Monte Carlo simulation [20]. On the other hand, using (26) and (27),

$$\frac{\text{area of triangle}}{\text{area of powder pattern}} = .0008.$$

Although the triangle is .08% of the area of the powder patten it accounts for 10% of the powder pattern intensity even in the situation where the triangle is very small. Points that are close together within the triangle can map back to distant points in the u,v plane, so points in the triangle are very sensitive to error in the determination of the peptide plane orientation.

3.2. The sweet spot

The point in the frequency plane where the intensity is smallest we call the *sweet spot*. The coordinates (σ, ν) of the sweet spot are found by finding the corresponding points in the (u, v) plane which maximize the denominator in (20),

$$|(b\,u + c\,v)u|\sqrt{1-u^2-v^2}. \quad (31)$$

Setting both partial derivatives equal to zero and solving using b and c from the above example, we get $(u, v) = (0.81, 0.08)$. This maps to the sweet spot $(\sigma, \nu) = (136, 5.26)$ (Fig. 5). A useful measure of relative error at a point in the frequency plane is the ratio of the intensity there to the intensity at the sweet spot.

3.3. Experimental data

As an application of the intensity analysis, we use PISEMA data from the M2 transmembrane domain of the proton channel (M2-TMD) [6]. The data for 14 out of the 18 transmembrane residues were obtained by PISEMA. These data are plotted in Fig. 5. The intensity ratio of each residue in the transmembrane region of M2 with respect to the sweet spot, I_r, is given in Fig. 6. Resonances for A29, I33, and L38 are clearly closest to the edge of the ellipse compared to resonances for other residues and hence they have a higher I_r.

The interpretation of the spectral frequencies from PISEMA data is dependent on solving the degeneracy problem which has been addressed here and elsewhere [16,17] and in specifically determining the resonance frequency, which may have a considerable linewidth. Linewidths can be inhomogeneous, reflecting a mosaic spread of orientation, or homogeneous reflecting efficient T_2 relaxation. We next examine the influence of mosaic spread and the component of linewidth due to mosaic spread.

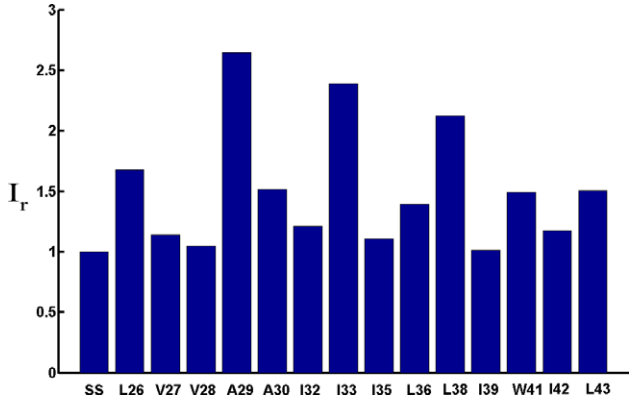

Fig. 6. Relative intensities for the M2 data points shown in Fig. 5. SS is the sweet spot. Here, the intensities were calculated using (21).

3.4. Mosaic spread or frequency dependent contributions to linewidth

Solid-state NMR experiments such as PISEMA are performed on aligned samples, and are subject to errors in alignment often characterized by a mosaic spread of orientations. There are a variety of reasons for such misalignment [23]. For membrane proteins the mosaic spread reflects the variation of $\mathbf{B}_0$ in the principal axis frame and can be interpreted as a maximum angle or as a probability distribution.

Mosaic spread of a membrane protein can be modeled by a probability distribution on the set of rotation matrices, each rotation representing a perturbation of the sample in the lab frame. The sample is assumed to be rigid, so that the same rotation is applied to each of the molecular frames in the sample. The rotation matrix is given as $R(\alpha,\beta,\gamma)$ in terms of Euler angles. A simple model for mosaic spread is obtained by taking a probability distribution of the form $p(\beta)\sin(\beta)\mathrm{d}\alpha\mathrm{d}\beta\mathrm{d}\gamma$, where p is a Gaussian distribution with mean 0 [24]. Another possibility is a uniform distribution of mean 0 obtained by choosing p to be a constant in the interval from 0 to ε. In these models the distribution of the angles α and γ is uniform.

For simplicity we choose p as above to be constant. The Z axis in the lab frame corresponds to the magnetic field direction so in each molecular frame $\mathbf{B}_0$ is distributed uniformly in a circle of spherical radius $\mathrm{d}s_{\mathbf{B}_0}$ about the average direction. An indication of the effect on the frequencies is obtained by looking at the image in the frequency plane of this circle. The image obtained is the *footprint* of the lineshape on the frequency plane. The values of $\mathrm{d}s_{\mathbf{B}_0}$ considered here were 2°, 4°, and 8°.

As Eq. (25) shows, the intensity is related to the range in chemical shift and dipolar frequency. Here we analyze the effect of mosaic spread for the M2-TMD data points. Unlike other contributions to the linewidths which may have a fixed magnitude in the PISEMA frequency plane, we assume a fixed mosaic spread on the unit sphere. Think of the mosaic spread of the aligned sample as a small circle of radius $\mathrm{d}s_{\mathbf{B}_0}$ on the unit sphere representing a range of values for $\mathbf{B}_0$. When a circle of radius $\mathrm{d}s_{\mathbf{B}_0}$ is mapped to the frequency plane the footprint of the lineshape has a nearly elliptical image (Fig. 7). Let $\mathrm{d}\tilde{\sigma}$ and $\mathrm{d}\tilde{\nu}$ denote the difference between the maximum and minimum values of $\tilde{\sigma}$ and $\tilde{\nu}$, respectively. These represent the linewidth, or in this case range in spectral intensity, in each dimension caused by the mosaic spread.

The linewidths scale approximately linearly with the degree spread in the spectral region, so that the linewidths for a 4° spread are approximately twice the linewidths for a 2° spread. An illustration involving three experimental data points and four simulated data points is shown in Fig. 7. We observe that among the recorded data points L38 has the largest chemical shift linewidth and the least dipolar linewidth, while W41 has the least chemical shift linewidth and V28 has the largest dipolar linewidth.

3.5. Frequency independent contributions to linewidth

While the contribution of mosaic spread to linewidths is dependent on the frequency position in the PISEMA frequency plane, there are other contributions that are independent or nearly independent of the frequency position in the plane. These latter homogeneous contributions can result in heterogeneous error bars in the interpretation of the dipolar splitting and chemical shift frequency. By considering two points in different intensity regions of the frequency plane but with the same linewidth (or error bars) in the chemical shift direction, we show in Fig. 8 that the corresponding error bars on the $\mathbf{B}_0$ unit sphere are quite different. We showed that a fixed mosaic spread angle resulted in large frequency ranges near the sweet spot. Similarly, a fixed frequency range for a resonance near the sweet spot results in a narrow orientational range on the $\mathbf{B}_0$ unit sphere compared to a resonance in a high intensity region of the PISEMA ellipse.

4. Conclusions

Structure determination by solid-state NMR requires finding the orientation of frames within the molecule with respect to $\mathbf{B}_0$. This is equivalent to finding the coordinates of $\mathbf{B}_0$ in the frames. The functions giving $\mathbf{B}_0$ in terms of the

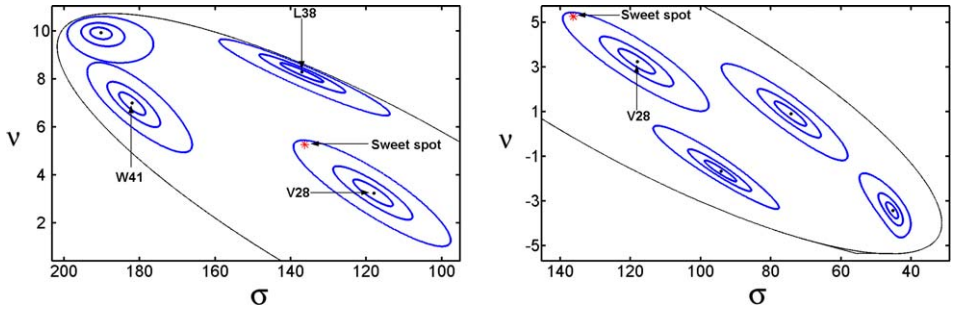

Fig. 7. Circles of radii 2°, 4°, and 8° on the $\mathbf{B}_0$ unit sphere are mapped into the PISEMA frequency plane for V28, L38, and W41 data points from M2-TMD, as well as a few simulated points in the top half and bottom half of the PISEMA ellipse. These show the effect of mosaic spread due to variations in sample alignment.

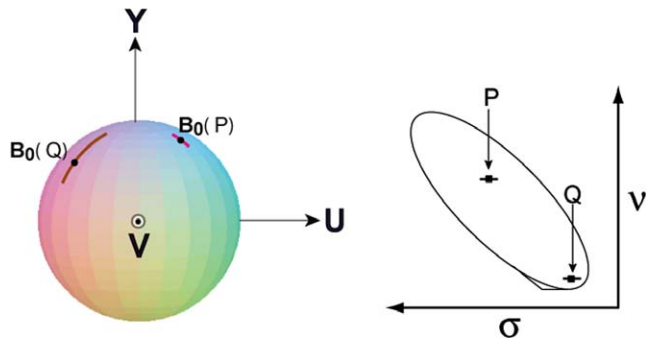

Fig. 8. Sensitivity to experimental errors of the coordinates on the $\mathbf{B}_0$ sphere of data points P and Q in the low and high intensity regions respectively of the PISEMA ellipse. Assume that these data points have a fixed experimental error bar of 5 ppm in their chemical shift measurements in the frequency plane. Let $\Delta\mathbf{B}_0(P)$ and $\Delta\mathbf{B}_0(Q)$ represent the error bars (arc length) on the $\mathbf{B}_0$ sphere of one out of the four possible unit magnetic field vectors corresponding to points P and Q. By computing $\Delta\mathbf{B}_0(P)$ and $\Delta\mathbf{B}_0(Q)$ we observe that the accuracy of the $\mathbf{B}_0$ coordinates depend on the position of the data points on the frequency plane. The coordinates of $\mathbf{B}_0$ is not reliable if the data point lies in a high intensity region since in this case $\Delta\mathbf{B}_0(Q)$ is large. However the coordinates of $\mathbf{B}_0$ is accurate if it lies in the low intensity region as seen by a relatively small $\Delta\mathbf{B}_0(P)$.

data can be differentiated, numerically or analytically, to determine how accurately the data determines the orientation. A change in $\mathbf{B}_0$ occurs corresponding to changes in the chemical shift and dipolar frequencies, and depends upon the location of the data point on the PISEMA frequency plane. In a 2D experiment such as PISEMA the equations are simple enough to obtain some expressions analytically and to easily calculate others numerically. The powder pattern intensity corresponds to the proportion of the area on the $\mathbf{B}_0$ sphere that maps onto a given frequency region. An analytical expression for the powder pattern intensity can be found easily. We have demonstrated that regions near the edge of the PISEMA ellipse and in the PISEMA triangle have higher intensities.

In aligned membrane peptides and protein samples mosaic spread values have been reported that range from $\pm 0.2°$ [25] to $\pm 10°$ [26]. While few of the observed PISEMA resonances have displayed images similar to Fig. 7, there have been very few examples of high signal to noise spectra. Higher magnetic field strengths and optimized radio frequency probes are dramatically improving PISEMA sensitivity, and consequently for those samples with significant mosaic spread it can be anticipated that such footprints of lineshapes will be observed in the future. In the absence of significant mosaic spread these will be dominated by other factors such as relaxation rates.

Importantly, it is the interpretation of the dipolar and chemical shift frequencies from the PISEMA spectra that leads to the characterization of protein backbone structure and alignment with respect to the membrane environment. From the analysis presented here it is possible to understand the lineshapes observed in the PISEMA spectra and the implication of these as orientational error bars.

Acknowledgments

J.R.Q. and T.A.C. were partially supported by NSF Grant DMS 9986036. M.S.C. was partially supported by NSF Grant DBI 9808098. R.B. and T.A. are partially supported by AHA Grant 0415075B. J.R.Q., R.B., M.S.C., and T.A.C. were partially supported by NIH Grant 1P01 GM64676.

References

[1] P.J. Wallin, G. Von Heijne, Genome-wide analysis of integral membrane proteins from eubacterial, archaean, and eukaryotic organisms, Protein Sci. 7 (1998) 1029–1038.
[2] T.A. Cross, J.R. Quine, Protein structure in anisotropic environments: development of orientational constraints, Concepts Magn. Reson. 12 (2000) 55–70.
[3] F.M. Marassi, S.J. Opella, NMR structural studies of membrane proteins, Curr. Opin. Struct. Biol. 8 (1998) 640–648.
[4] R. Fu, T.A. Cross, Solid state NMR investigation of protein and polypeptide structure, Annu. Rev. Biophys. Biomol. Struct. 28 (1999) 235–268.
[5] R.R. Ketchem, W. Hu, T.A. Cross, High resolution conformation of gramicidin A in a lipid bilayer by solid state NMR, Science 261 (1993) 1457–1460.
[6] J. Wang, S. Kim, F. Kovacs, T.A. Cross, Structure of the transmembrane region of the M2 protein H^+ channel, Protein Sci. 10 (2001) 2241–2250.
[7] Y. Kim, K. Valentine, S.J. Opella, S.L. Schendel, W.A. Cramer, Solid-state NMR studies of the membrane-bound closed state of the colicin E1 channel domain in lipid bilayers, Protein Sci. 7 (1998) 342–348.
[8] F.M. Marassi, J.J. Gesell, A.P. Valente, Y. Kim, M. Oblatt-Montal, M. Montal, S.J. Opella, Dilute spin-exchange assignment of solid-state NMR spectra of oriented proteins: acetylcholine M2 in bilayers, J. Biomol. NMR 14 (1999) 141–148.
[9] K. Nishimura, S. Kim, L. Zhang, T.A. Cross, The closed state of a H^+ channel helical bundle combining precise orientational and distance restraints from solid state NMR, Biochemistry 41 (2002) 13170–13177.
[10] S.H. Park, A.A. Mrse, A.A. Nevzorov, M.F. Mesleh, M. Oblatt-Montal, M. Montal, S.J. Opella, Three-dimensional structure of the channel-forming trans-membrane domain of virus protein "u" (Vpu) from HIV-1, J. Mol. Biol. 333 (2003) 409–424.
[11] Z. Song, F.A. Kovacs, J. Wang, J.K. Denny, S.C. Shekar, J.R. Quine, T.A. Cross, Transmembrane domain of M2 protein from influenza A virus studied by solid-state ^{15}N polarization inversion spin exchange at magic angle NMR, Biophys. J. 79 (2000) 767–775.
[12] C.H. Wu, A. Ramamoorthy, S.J. Opella, High-resolution heteronuclear dipolar solid-state NMR spectroscopy, J. Magn. Reson. 109 (1994) 270–282.
[13] A. Ramamoorthy, Y. Wei, D. Lee, PISEMA solid state NMR spectroscopy, Ann. Reports on NMR Spectrosc. 52 (2004) 1–52.
[14] M. Linder, A. Höhener, R.R. Ernst, Orientation of tensorial interactions determined from two-dimensional NMR powder spectra, J. Chem. Phys. 73 (1980) 4959–4970.
[15] J.R. Quine, T.A. Cross, Protein structure in anisotropic environments: unique structural fold from orientational constraints, Concepts Magn. Reson. 12 (2000) 71–82.
[16] J. Denny, J. Wang, T.A. Cross, J.R. Quine, PISEMA powder patterns and PISA wheels, J. Magn. Reson. 152 (2001) 217–226.
[17] F.A. Marassi, S.J. Opella, Using PISA pies to resolve ambiguities in angular constraints from PISEMA spectra of aligned proteins, J. Biomol. NMR 23 (2002) 239–242.
[18] W. Mai, W. Hu, C. Wang, T.A. Cross, Orientational constraints as three-dimensional structure constraints from chemical shift anisotro-

py-the polypeptide backbone of gramicidin-A in a lipid bilayer, Protein Sci. 2 (1993) 532–542.
[19] J. Wang, J. Denny, C. Tian, S. Kim, Y. Mo, F. Kovacs, Z. Song, K. Nishimura, Z. Gan, R. Fu, J.R. Quine, T.A. Cross, Imaging membrane protein helical wheels, J. Magn. Reson. 144 (2000) 162–167.
[20] R. Bertram, T. Asbury, F. Fabiola, J.R. Quine, T.A. Cross, M.S. Chapman, Atomic refinement with correlated solid-state NMR restraints, J. Magn. Reson. 163 (2003) 300–309.
[21] J.R. Quine, T.A. Cross, M.S. Chapman, R. Bertram, Mathematical aspects of protein structure determination with NMR orientational restraints, Bull. Math. Biol. 66 (2004) 1705–1730.
[22] Q. Teng, M. Iqbal, T.A. Cross, Determination of the ^{13}C chemical shift and ^{14}N electric field gradient tensor orientations with respect to the molecular frame in a polypeptide, J. Am. Chem. Soc. 114 (1992) 5312–5321.
[23] F. Moll III, T.A. Cross, Optimizing and characterizing alignment of oriented lipid bilayers containing gramicidin D, Biophys. J. 57 (1990) 351–362.
[24] A.A. Nevzorov, S. Moltke, M.P. Heyn, M.F. Brown, Solid-state NMR line shapes of uniaxially oriented immobile systems, J. Am. Chem. Soc. 121 (1999) 7636–7643.
[25] W. Hu, K.-C. Lee, T.A. Cross, Tryptophans in membrane proteins : indole ring orientations and functional implications in the gramicidin channel, Biochemistry 32 (1993) 7035–7047.
[26] S.K. Straus, W.R.P. Scott, A. Watts, Assessing the effects of time and spatial averaging in ^{15}N chemical shift/^{15}N–^{1}H dipolar correlation solid state NMR experiments, J. Biomol. NMR 26 (2003) 283–295.